REPORT DOCUMENTATION PAGE

Form Approved
OMB No. 0704-0188

1. AGENCY USE ONLY *(Leave blank)*	2. REPORT DATE	3. REPORT TYPE AND DATES COVERED
	August 1992	Technical Paper

4. TITLE AND SUBTITLE
Analysis and Prediction of Multiple-Site Damage (MSD) Fatigue Crack Growth

5. FUNDING NUMBERS
WU 505-63-50-04

6. AUTHOR(S)
D. S. Dawicke and J. C. Newman, Jr.

7. PERFORMING ORGANIZATION NAME(S) AND ADDRESS(ES)
NASA Langley Research Center
Hampton, VA 23681-0001

8. PERFORMING ORGANIZATION REPORT NUMBER
L-17006

9. SPONSORING/MONITORING AGENCY NAME(S) AND ADDRESS(ES)
National Aeronautics and Space Administration
Washington, DC 20546-0001

10. SPONSORING/MONITORING AGENCY REPORT NUMBER
NASA TP-3231

11. SUPPLEMENTARY NOTES
D. S. Dawicke: Analytical Services & Materials, Inc., Hampton, VA.
J. C. Newman, Jr.: Langley Research Center, Hampton, VA.

12a. DISTRIBUTION/AVAILABILITY STATEMENT
Unclassified–Unlimited

Subject Category 39

12b. DISTRIBUTION CODE

13. ABSTRACT *(Maximum 200 words)*
A technique was developed to calculate the stress intensity factor for multiple interacting cracks. The analysis was verified through comparison with accepted methods of calculating stress intensity factors. The technique was incorporated into a fatigue crack growth prediction model and used to predict the fatigue crack growth life for multiple-site damage (MSD). The analysis was verified through comparison with experiments conducted on uniaxially loaded flat panels with multiple cracks. Configurations with nearly equal and unequal crack distributions were examined. The fatigue crack growth predictions agreed within 20 percent of the experimental lives for all crack configurations considered.

14. SUBJECT TERMS
Multiple-site damage; Stress intensity factor; Fatigue; Life prediction; Indirect boundary element

15. NUMBER OF PAGES
16

16. PRICE CODE
A03

17. SECURITY CLASSIFICATION OF REPORT	18. SECURITY CLASSIFICATION OF THIS PAGE	19. SECURITY CLASSIFICATION OF ABSTRACT	20. LIMITATION OF ABSTRACT
Unclassified	Unclassified		

Abstract

A technique was developed to calculate the stress intensity factor for multiple interacting cracks. The analysis was verified through comparison with accepted methods of calculating stress intensity factors. The technique was incorporated into a fatigue crack growth prediction model and used to predict the fatigue crack growth life for multiple-site damage (MSD). The analysis was verified through comparison with experiments conducted on uniaxially loaded flat panels with multiple cracks. Configurations with nearly equal and unequal crack distributions were examined. The fatigue crack growth predictions agreed within 20 percent of the experimental lives for all crack configurations considered.

Introduction

The continued structural integrity of the aging commercial transport aircraft fleet is of great concern to the aerospace community. The long service life of these aircraft increases the possibility of a reduction or loss of structural integrity due to fatigue cracking. Multiple-site damage (MSD), in particular, is one form of fatigue cracking that presents special problems to the aircraft maintenance operator as well as to the structural analyst. MSD refers to the occurrence of several cracks close enough together to influence each other and to affect the overall structural integrity. The critical crack size for individual cracks may be relatively small, making their detection with existing nondestructive examination (NDE) methods difficult. The mutual influence of the adjacent cracks increases the complexity of predicting fatigue crack growth behavior.

The linear elastic fracture mechanics (LEFM) approach to predicting fatigue crack growth relates the stress intensity factor to the crack growth rate. Stress intensity factors can be calculated with a variety of analytical and numerical techniques. Closed form solutions generally exist for a limited number of simple cases such as infinite plate problems (ref. 1). Numerical techniques such as finite element or boundary element analyses are often used for more complex crack configurations (ref. 2). However, the large number of crack tips potentially involved in analyzing an MSD problem would require extensive computer resources using finite element analyses. Boundary force techniques (ref. 3) require less modeling effort, but can only model one crack. Approximate solutions of MSD stress intensity factors were developed by combining known solutions (refs. 4 and 5).

Numerical techniques could be used to calculate stress intensity factors for the entire fatigue crack growth life. However, the scale of modeling required to capture the effect of both the local structural details and the large-scale structural details would be prohibitive in a life analysis where the stress intensity factors are calculated many times as the cracks grow. A more practical approach would be to consider what influences the crack growth behavior at different stages of life. The damage tolerant life of a structural component susceptible to MSD cracking can be divided into three regions of crack growth: local, MSD, and post-linkup. The local crack growth region consists of the initial development of cracks at a local structural detail, such as a rivet hole. The cracks are strongly influenced by the local structural details, but are too small to have a large influence on adjacent cracks. The cracks in the MSD region are strongly influenced by the adjacent cracks. The crack in the post-linkup region behaves as a single long crack influenced by the large-scale structural details.

The technique described in this paper examines the crack growth life for the local and MSD regions of crack growth. The post-linkup region was not considered and would require large-scale analyses of structural details, such as stringers, cutouts, and riveted connections, using finite element shell codes. An alternating indirect boundary element (AIBE) technique was developed herein to calculate the stress intensity factor for multiple interacting cracks. A hole correction factor was added to the AIBE solution to reduce the detail of modeling required. This technique was sufficiently fast and accurate to be incorporated into a fatigue crack growth prediction code.

This paper describes the AIBE technique of determining stress intensity factors. The technique was verified by comparisons of the calculated stress intensity factors with those determined from accepted solutions, finite element methods, and boundary element methods. Damage tolerant life predictions were made with the AIBE technique in conjunction with a hole correction factor. The life predictions were compared with MSD tests conducted on flat 2024-T3 aluminum alloy specimens with multiple cracks propagating from a line of open holes.

Symbols

a	half crack length
BFM	boundary force method
C	constant
d	half centerline distance between holes
d_j	half element length

K	stress intensity factor
N_p	number of cycles, predicted
N_t	number of cycles, test
R	stress ratio
S	applied stress
s	integration variable
w	half specimen width
α	constraint
σ_o	flow stress
σ_n	normal stress
τ	shear stress

Stress Intensity Factor Calculations

The use of linear elastic fracture mechanics to predict fatigue crack growth behavior requires the determination of the stress intensity factor. The stress intensity factor is influenced by geometric considerations such as crack length, other adjacent cracks, free boundaries, and holes. The various geometric considerations will affect the stress intensity factor differently as the crack grows. Consider, for example, cracks propagating out of two open holes in an infinite body, as shown in figure 1. The influence of the hole is large when the ratio of half crack length to hole radius a/r is small and then decreases as a/r increases, while the influence of the adjacent crack steadily increases, as shown in figure 2.

The growth of multiple cracks in a structure can be divided into three regions, each of which is governed by different geometric considerations. The stress intensity factor of cracks in the local crack growth region is strongly influenced by the local structural details. The cracks in this region are small, as would be the influence of any small adjacent cracks. The stress intensity factors of cracks in the MSD crack growth region are strongly influenced by the adjacent cracks, and the effects of local structural details diminish. The post-linkup region is influenced strongly by large-scale structural details.

An alternating indirect boundary element (AIBE) method was developed to calculate the stress intensity factor for multiple interacting cracks. A correction factor was applied to the stress intensity factor to account for the local structural details. Consideration of the post-linkup region was not required for the structural configuration examined. The following sections describe the AIBE technique and the hole correction factor.

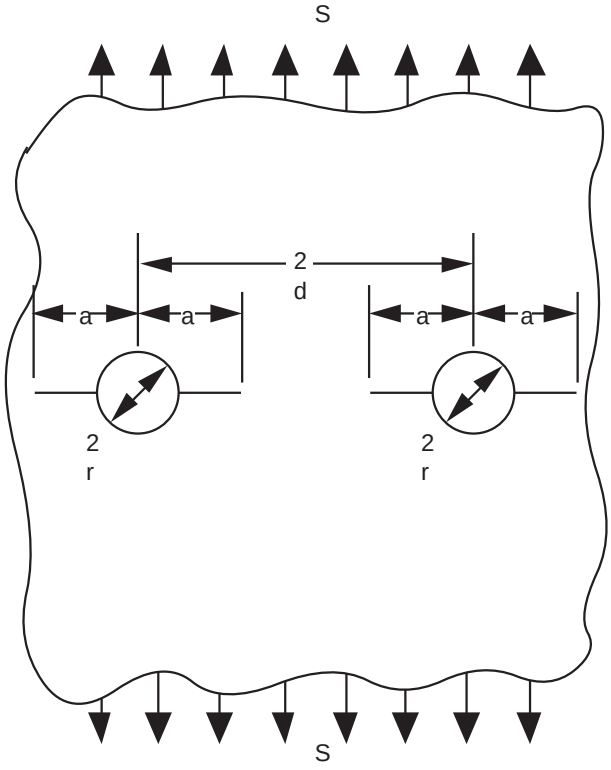

Figure 1. Cracks propagating from two sides of two holes in an infinite plate subjected to uniaxial loading.

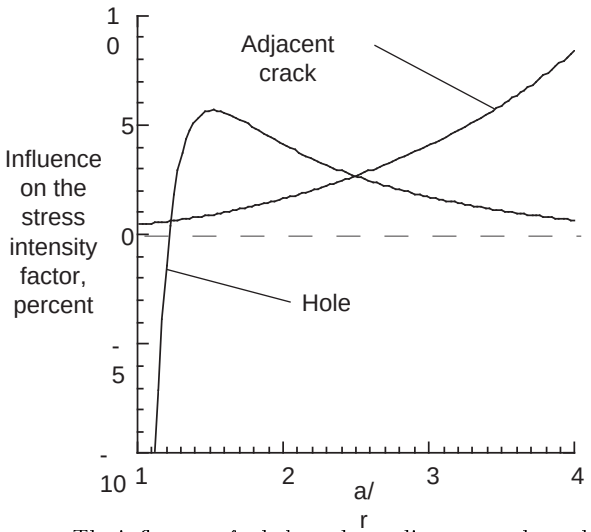

Figure 2. The influence of a hole and an adjacent crack on the stress intensity factor for the cracks illustrated in figure 1 ($r/d = 0.15$).

Alternating Indirect Boundary Element (AIBE) Method

The stress intensity factors for multiple interacting cracks were calculated with an alternating indirect boundary element (AIBE) technique. The

AIBE method is based on the principle of superposition of stresses associated with cracks and free (or loaded) boundaries. To illustrate the superposition of stresses, consider a single crack in a semi-infinite sheet, as shown in figure 3. (An MSD configuration would be obtained by adding additional cracks and free boundaries.) Figure 4 illustrates how superposition was used to determine the stress functions for a crack in a semi-infinite sheet. The cracked infinite sheet with a uniform crack-face stress S is shown in figure 4(b). The uncracked infinite sheet subjected to a uniform remote stress S is shown in figure 4(c). Figure 4(d) shows the uncracked sheet with the nonuniform stresses $\sigma_x^b(y)$ and $\tau_{xy}^b(y)$ acting on a line that corresponds to the free boundary and the nonuniform stresses $\sigma_x^c(x)$ and $\tau_{xy}^c(x)$ acting along $y = 0, |x| < a$. The crack-face loading (fig. 4(e)) is superimposed on the uncracked loading (fig. 4(d)) to produce the stress-free crack face shown in figure 4(a).

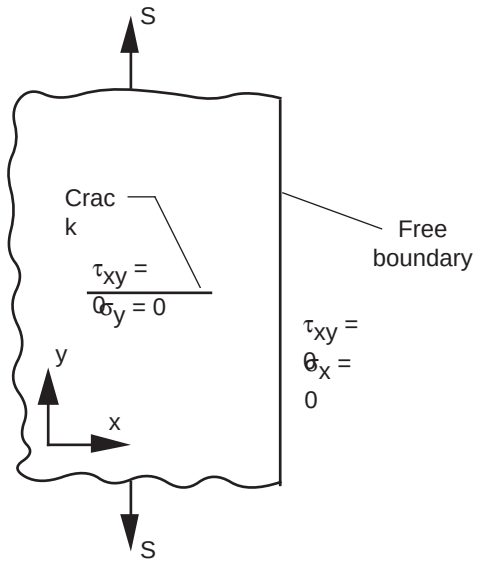

Figure 3. Semi-infinite body with crack.

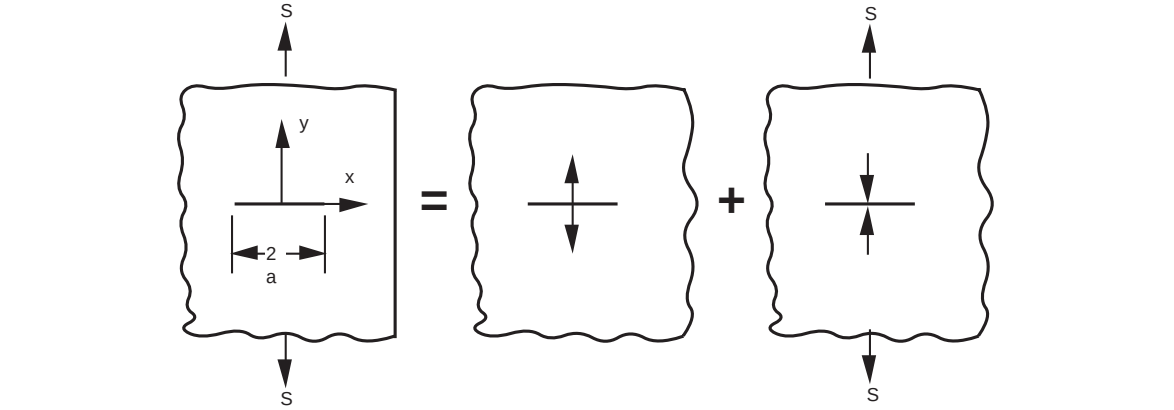

(a) Cracked semi-infinite sheet with remote stress S.

(b) Cracked infinite sheet with uniform crack-face stress.

(c) Uncracked infinite sheet with uniform remote stress.

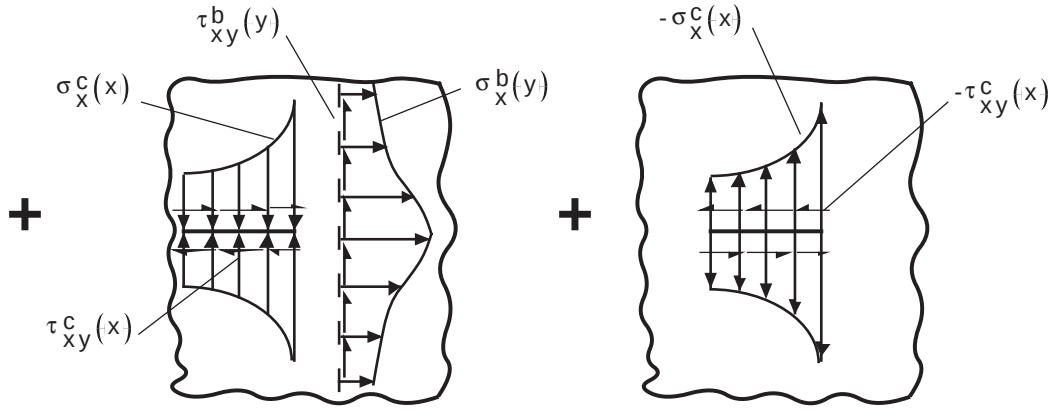

(d) Uncracked infinite sheet with nonuniform stresses acting along free boundary and along $y = 0, |x| < a$.

(e) Infinite sheet with crack-face loading.

Figure 4. Principle of superposition applied to a crack in a semi-infinite plate.

The formulation requires analytical expressions for the stresses due to the loadings shown in figures 4(d) and 4(e). Analytical expressions developed by Timoshenko and Goodier (ref. 6), Westergaard (refs. 7), and Tada and Irwin (ref. 8) were used to formulate the necessary expressions for the stress distribution.

Uncracked infinite sheet with nonuniform line loading. The analytical expressions defined by Timoshenko and Goodier (ref. 6) for the stresses at any point (x, y) due to a concentrated force on an infinite body were used to formulate the equations for the stresses in an uncracked infinite sheet with a nonuniform line loading (fig. 4(d)). In the Timoshenko and Goodier expressions, the concentrated force is applied at the origin of the local coordinate system (x, y), as illustrated in figure 5. The stresses due to a force P acting in the x-direction are given by:

$$\sigma_x = \frac{P}{2\pi}\frac{x}{x^2+y^2}\left[-(3+\nu)+2(1+\nu)\frac{y^2}{x^2+y^2}\right] \quad (1)$$

$$\sigma_y = \frac{P}{2\pi}\frac{x}{x^2+y^2}\left[(1-\nu)-2(1+\nu)\frac{y^2}{x^2+y^2}\right] \quad (2)$$

$$\tau_{xy} = \frac{-P}{2\pi}\frac{y}{x^2+y^2}\left[(1-\nu)+2(1+\nu)\frac{x^2}{x^2+y^2}\right] \quad (3)$$

The stresses due to a force Q acting in the y-direction are given by

$$\sigma_x = \frac{Q}{2\pi}\frac{y}{x^2+y^2}\left[(1-\nu)-2(1+\nu)\frac{x^2}{x^2+y^2}\right] \quad (4)$$

$$\sigma_y = \frac{Q}{2\pi}\frac{y}{x^2+y^2}\left[-(3+\nu)+2(1+\nu)\frac{x^2}{x^2+y^2}\right] \quad (5)$$

$$\tau_{xy} = \frac{-Q}{2\pi}\frac{x}{x^2+y^2}\left[(1-\nu)+2(1+\nu)\frac{y^2}{x^2+y^2}\right] \quad (6)$$

where ν is Poisson's ratio. The stresses due to normal and shear stress distributions were obtained by dividing the boundary into discrete elements and integrating equations (1)–(6) over each element length $(2d_j)$, as illustrated in figure 6. The stresses due to a normal stress distribution $\sigma_n(s)$ are given by

$$\sigma_x = \frac{1}{2\pi}\int_{-d_j}^{d_j}\frac{x\sigma_n(s)}{x^2+(y+s)^2}\left[-(3+\nu)+2(1+\nu)\frac{(y+s)^2}{x^2+(y+s)^2}\right]ds \quad (7)$$

$$\sigma_y = \frac{1}{2\pi}\int_{-d_j}^{d_j}\frac{x\sigma_n(s)}{x^2+(y+s)^2}\left[(1-\nu)-2(1+\nu)\frac{(y+s)^2}{x^2+(y+s)^2}\right]ds \quad (8)$$

$$\tau_{xy} = \frac{-1}{2\pi}\int_{-d_j}^{d_j}\frac{(y+s)\sigma_n(s)}{x^2+(y+s)^2}\left[(1-\nu)+2(1+\nu)\frac{x^2}{x^2+(y+s)^2}\right]ds \quad (9)$$

where $\sigma_n(s)$ is assumed to have a quadratic form as

$$\sigma_n(s) = C_0 + C_1 s + C_2 s^2 \quad (10)$$

The stresses due to a shear stress distribution $\tau(s)$ are given by

$$\sigma_x = \frac{1}{2\pi}\int_{-d_j}^{d_j}\frac{(y+s)\tau(s)}{x^2+(y+s)^2}\left[(1-\nu)-2(1+\nu)\frac{x^2}{x^2+(y+s)^2}\right]ds \quad (11)$$

$$\sigma_y = \frac{1}{2\pi}\int_{-d_j}^{d_j}\frac{(y+s)\tau(s)}{x^2+(y+s)^2}\left[-(3+\nu)+2(1+\nu)\frac{x^2}{x^2+(y+s)^2}\right]ds \quad (12)$$

$$\tau_{xy} = \frac{-1}{2\pi}\int_{-d_j}^{d_j}\frac{x\tau(s)}{x^2+(y+s)^2}\left[(1-\nu)+2(1+\nu)\frac{(y+s)^2}{x^2+(y+s)^2}\right]ds \quad (13)$$

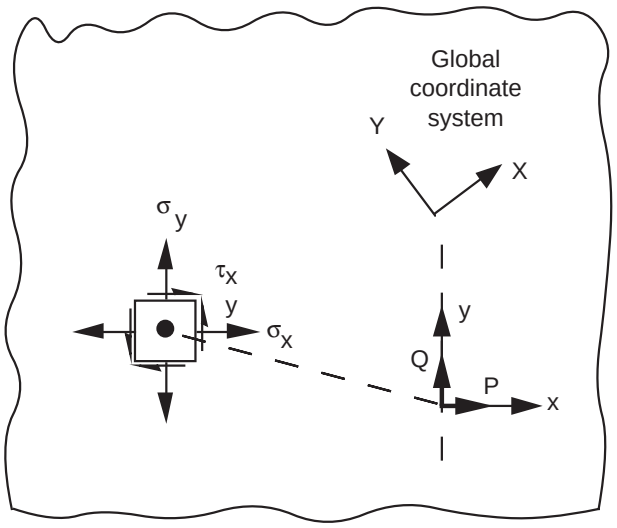

Figure 5. Concentrated forces P and Q in an infinite body.

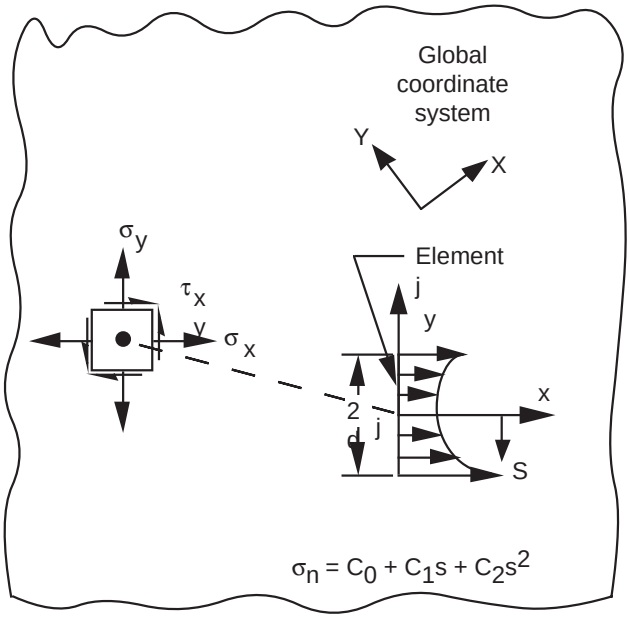

Figure 6. A line element with a quadratic normal stress distribution for an infinite body (note that a similar procedure is used for the shear stresses).

where $\tau(s)$ is assumed to have a quadratic form as

$$\tau\,(s) = D_0 + D_1 s + D_2 s^2 \tag{14}$$

where C_i and D_i $(i = 0, 1, 2)$ are known for each element and will be discussed later. A coordinate transformation is performed on the calculated stresses to be consistent with the global coordinate system (X, Y).

Cracked infinite sheet with nonuniform crack-face loading. From Westergaard (ref. 7), the stresses in an infinite sheet with crack-face loadings can be written in terms of two stress functions, Z_I and Z_{II}, as follows:

$$\sigma_x = \mathrm{Re}\, Z_I - y\,\mathrm{lm}\,\frac{dZ_I}{dz} + 2\,\mathrm{lm}\, Z_{II} + y\,\mathrm{Re}\,\frac{dZ_{II}}{dz} \tag{15}$$

$$\sigma_y = \mathrm{Re}\, Z_I + y\,\mathrm{lm}\,\frac{dZ_I}{dz} - y\,\mathrm{Re}\,\frac{dZ_{II}}{dz} \tag{16}$$

$$\tau_{xy} = -y\,\mathrm{Re}\,\frac{dZ_I}{dz} + \mathrm{Re}\, Z_{II} - y\,\mathrm{lm}\,\frac{dZ_{II}}{dz} \tag{17}$$

The Westergaard stress functions, Z_I and Z_{II}, are defined for point forces P and Q acting on a crack of length $2a$, as illustrated in figure 7.

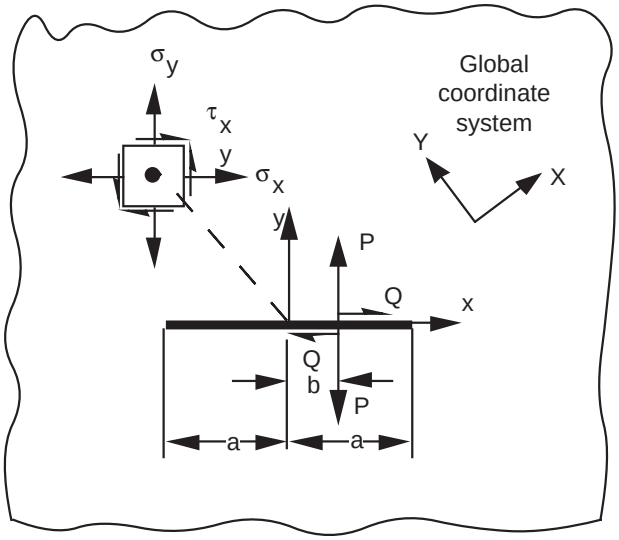

Figure 7. Concentrated forces P and Q acting on a crack in an infinite body.

$$Z_I\,(z) = \frac{P}{\pi}\,\frac{\sqrt{a^2 - b^2}}{(z-b)\,\sqrt{z^2 - a^2}} \tag{18}$$

$$Z_{II}\,(z) = \frac{Q}{\pi}\,\frac{\sqrt{a^2 - b^2}}{(z-b)\,\sqrt{z^2 - a^2}} \tag{19}$$

where $z = x + iy$.

The stress functions for crack-face stress distributions were obtained by dividing the crack into discrete elements and integrating equations (18) and (19) over the length of each crack element $(2d_j)$, as illustrated in figure 8. The resulting stress functions for each element are given by

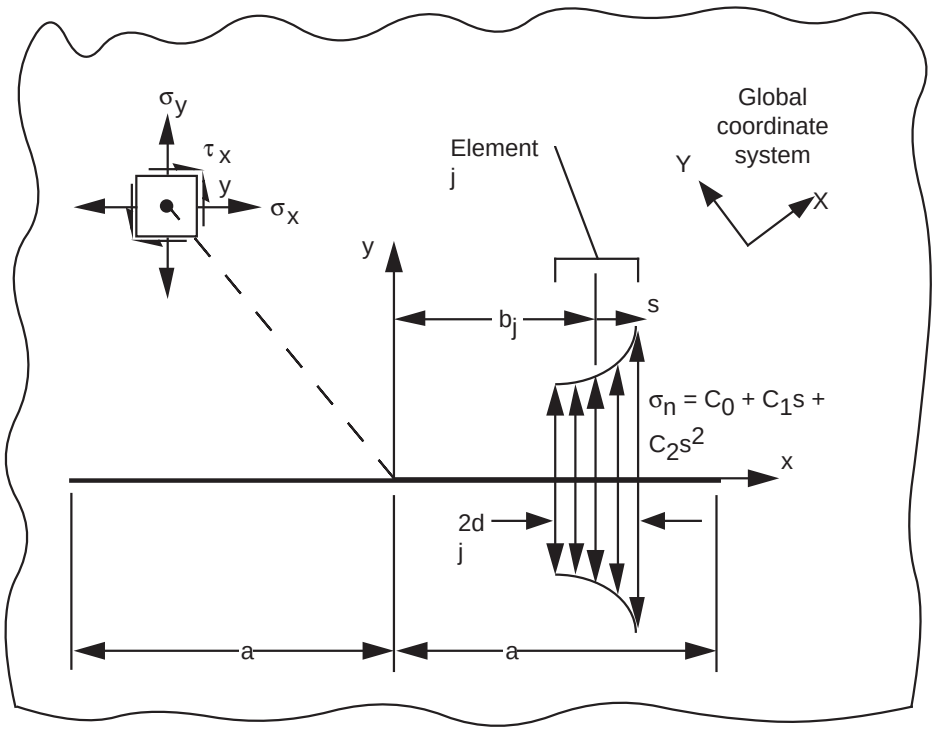

Figure 8. A crack element with a quadratic normal stress distribution for a crack in an infinite body (note that a similar procedure is used for the shear stresses).

$$Z_I(z) = \frac{1}{\pi}\int_{-d_j}^{d_j} \sigma_n(s)\,\frac{\sqrt{a^2-(b_j+s)^2}}{(z-b_j-s)\sqrt{z^2-a^2}}\,ds \qquad (20)$$

$$Z_{II}(z) = \frac{1}{\pi}\int_{-d_j}^{d_j} \tau(s)\,\frac{\sqrt{a^2-(b_j+s)^2}}{(z-b_j-s)\sqrt{z^2-a^2}}\,ds \qquad (21)$$

Equations (19) and (20) could theoretically be integrated exactly, but numerical integration proved to be computationally efficient. A coordinate transformation was performed on the calculated stresses to be consistent with the global coordinate system (X, Y).

Stress intensity factor equations. The mode I and mode II stress intensity factors due to concentrated loads P and Q on a crack in an infinite body (refs. 7 and 8) are given by

$$K_I = \frac{P}{\sqrt{\pi a}}\sqrt{\frac{a+b}{a-b}} \qquad (22)$$

$$K_{II} = \frac{Q}{\sqrt{\pi a}}\sqrt{\frac{a+b}{a-b}} \qquad (23)$$

The stress intensity factors for a crack face stress distribution are determined by integrating equations (22) and (23) over the length of each crack element $(2d_j)$ measured with respect to the distance from the element centroid to the center of the crack (b_j), as

$$K_I = \int_{b_j-d_j}^{b_j+d_j} \frac{1}{\sqrt{\pi a}}\sigma_n(s)\sqrt{\frac{a+s}{a-s}}\,ds \qquad (24)$$

$$K_{II} = \int_{b_j-d_j}^{b_j+d_j} \frac{1}{\sqrt{\pi a}}\tau(s)\sqrt{\frac{a+s}{a-s}}\,ds \qquad (25)$$

The total stress intensity factor solutions are obtained by adding the contributions from each crack element.

MSD configurations. A two-dimensional cracked structure can be modeled with the alternating indirect boundary element (AIBE) method by describing the cracks and external boundaries with a series of line segments or elements. The boundaries must be continuous and the cracks contained within the boundaries and not intersecting other cracks. The quadratic elemental stress distribution was used to reduce the number of elements (i.e., the number of degrees of freedom) required to describe a crack

problem. The quadratic stress distributions require that the stresses be defined at three nodal points in each element, $s = -0.6d_j$, 0, and $0.6d_j$. The solution is obtained by first assuming initial values of the six stress coefficients (eqs. (10) and (14)) of each element. The initial value is not crucial, a value of unity for each coefficient is sufficient for convergence, but using the results from a previous solution (when available) will considerably reduce the number of iterations. The stresses for each element (three normal and three shear stresses) are determined with the current stress coefficients and assembled into a vector of length $6n$, where n is the total number of elements, as

$$\left\{\sigma^{\text{old}}\right\} = \begin{Bmatrix} \vdots \\ \tau\left(0.6d_{i-1}\right) \\ \sigma_n\left(-0.6d_i\right) \\ \tau\left(-0.6d_i\right) \\ \sigma_n\left(0\right) \\ \tau\left(0\right) \\ \sigma_n\left(0.6d_i\right) \\ \tau\left(0.6d_i\right) \\ \sigma_n\left(-0.6d_{i+1}\right) \\ \vdots \end{Bmatrix} = \begin{Bmatrix} \vdots \\ D_0^{i-1} + D_1^{i-1}\left(0.6d_{i-1}\right) + D_2^{i-1}\left(0.6d_{i-1}\right)^2 \\ C_0^i + C_1^i\left(-0.6d_i\right) + C_2^i\left(-0.6d_i\right)^2 \\ D_0^i + D_1^i\left(-0.6d_i\right) + D_2^i\left(-0.6d_i\right)^2 \\ C_0^i \\ D_0^i \\ C_0^i + C_1^i\left(0.6d_i\right) + C_2^i\left(0.6d_i\right)^2 \\ D_0^i + D_1^i\left(0.6d_i\right) + D_2^i\left(0.6d_i\right)^2 \\ C_0^{i+1} + C_1^{i+1}\left(-0.6d_{i+1}\right) + C_2^{i+1}\left(-0.6d_{i+1}\right)^2 \\ \vdots \end{Bmatrix} \tag{26}$$

An influence matrix $[t]$ is formed using equations (7)–(17) to determine the effect of the stresses $\{\sigma^{\text{old}}\}$ of element i on the stresses $\{\sigma^{\text{new}}\}$ at element j. The influence matrix is a fully populated, nonsymmetric $6n \times 6n$ matrix. The new elemental stresses are defined such that the imposed stress constraints $\{\sigma^{\text{imposed}}\}$ are satisfied, as given by

$$\{\sigma^{\text{new}}\} = \left\{\sigma^{\text{imposed}}\right\} - [t]\left\{\sigma^{\text{old}}\right\} \tag{27}$$

The imposed stress constraints $\{\sigma^{\text{imposed}}\}$ are either zero for stress-free boundaries and cracks or the applied stresses. Once the stress distributions $\{\sigma^{\text{new}}\}$ are calculated, the stress intensity factors are calculated with equations (24) and (25).

The process is repeated until the stress intensity factor solution converges, typically defined as changes of less than 0.5 percent. The solution could be obtained directly by inverting $[t]$, as given by

$$\{\sigma^{\text{new}}\} = \left[t^{-1}\right]\left\{\sigma^{\text{imposed}}\right\} \tag{28}$$

However, the iteration method was more efficient for use in a life prediction code, which requires repeated stress intensity factor solutions for a large number of crack lengths. Rapid convergence of the solution is obtained if the stress coefficients from the previous crack lengths are used as the initial values in the current calculation.

Local Correction Factor

The stress intensity factor for cracks in the local growth region is strongly influenced by local structural details. To describe these details explicitly would add considerably to the size of the required MSD model. Alternatively, one structural detail could be modeled accurately, and a simple relationship describing its influence on the stress intensity factor could be developed. Such a relationship could be incorporated into the MSD stress intensity factor calculations.

One structural detail that has been extensively analyzed is an open hole. The stress intensity factor for cracks propagating from opposite sides of an open hole in an infinite plate can be written as

$$K = S\sqrt{\pi a}F_h\left(\frac{a}{r}\right) \tag{29}$$

$$F_h\left(\frac{a}{r}\right) = \sqrt{1-\frac{r}{a}}\left[1.0 + 0.358\frac{r}{a} + 1.425\left(\frac{r}{a}\right)^2 - 1.578\left(\frac{r}{a}\right)^3 + 2.156\left(\frac{r}{a}\right)^4\right] \tag{30}$$

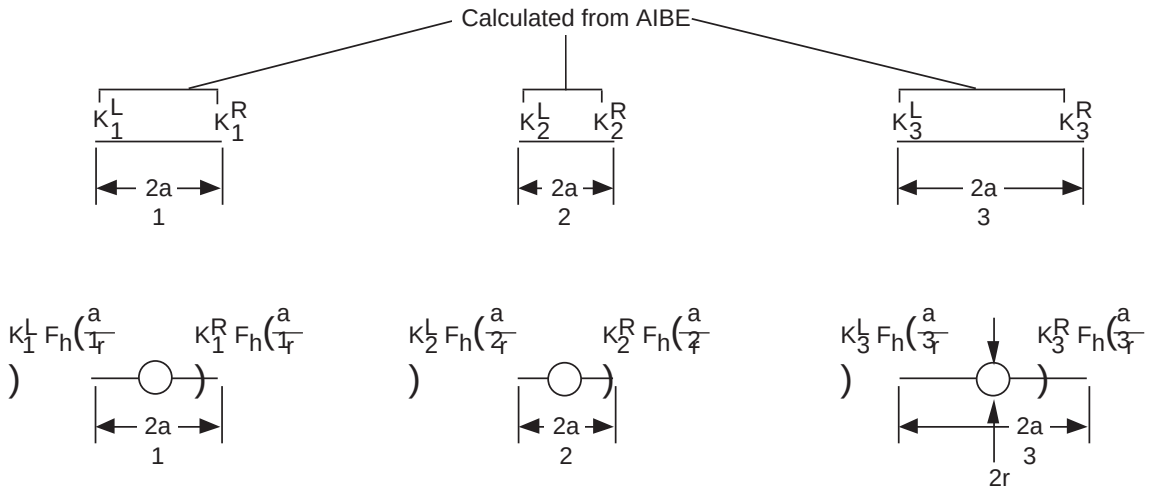

Figure 9. Illustration of use of the hole correction factor $F_h(\frac{a}{r})$ for cracks emanating from circular holes.

where r is the hole radius, S is the applied stress, a is the half crack length, and $F_h\left(\frac{a}{r}\right)$ is the hole correction factor (ref. 9). The stress intensity factors for a series of cracks emanating from a row of holes would be the products of the hole correction factor for each hole and the stress intensity factor for each crack, as illustrated in figure 9.

Stress Intensity Factor Verification

The AIBE technique was verified by comparing the stress intensity factors calculated by AIBE with those from an accepted solution, a boundary force analysis, and finite element analyses. The crack configurations used both a single center crack and multiple cracks in a finite body. The use of the local correction factor was examined by considering cracks propagating from two holes.

AIBE Stress Intensity Factor Verification

A center crack tension (CCT) panel subjected to uniaxial loading perpendicular to the plane of the crack was analyzed. The crack was divided into 12 elements, with smaller element lengths near the crack tip, as shown in figure 10. The boundary mesh consisted of 72 elements, with smaller element lengths near the corners and the edges closest to the crack tip. (The symmetry of the configuration was not used to reduce the model.) The variation in element sizes was necessary to account for the steep gradients in the required balancing stresses that occur at points of discontinuity in the boundary and are not necessarily associated with steep gradients in physical stresses. An accepted solution for the stress intensity factor for a CCT specimen is given by Fedderson in reference 10 as

$$K = S\sqrt{\pi a \sec\left(\frac{\pi a}{2w}\right)} \tag{31}$$

The stress intensity factor results from the AIBE analysis agreed with the accepted solution within 1 percent for crack length-to-width ratios (a/w) below 0.8, as shown in figure 11.

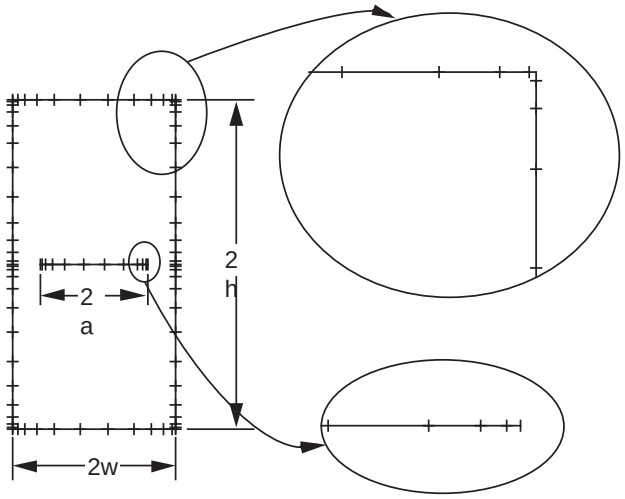

Figure 10. AIBE mesh used in the analysis of a center crack tension specimen. $h/w = 2$.

A centered, inclined crack subjected to uniaxial loading was also analyzed. The crack length was constant with $a/w = 1/3$, and the orientation of the crack with respect to the direction of loading was varied from $\theta = 0°$ to $85°$ ($\theta = 0°$ being perpendicular to the direction of loading). The mode I and mode II stress intensity factors were calculated with

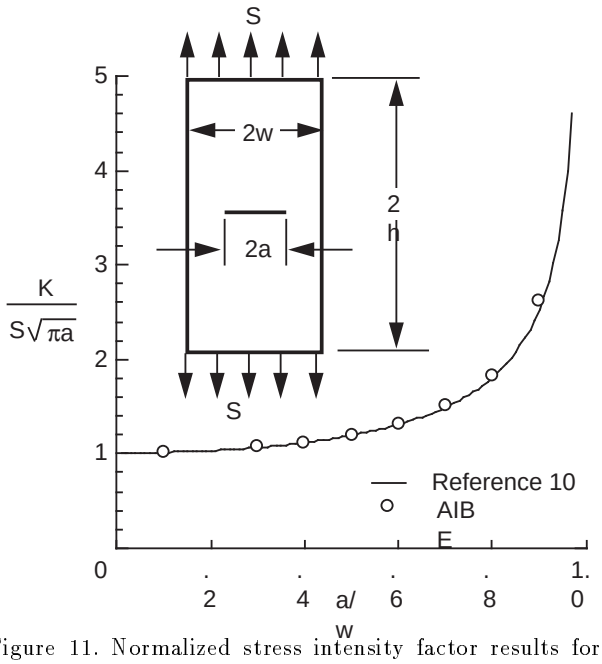

Figure 11. Normalized stress intensity factor results for a CCT specimen. $h/w = 2$.

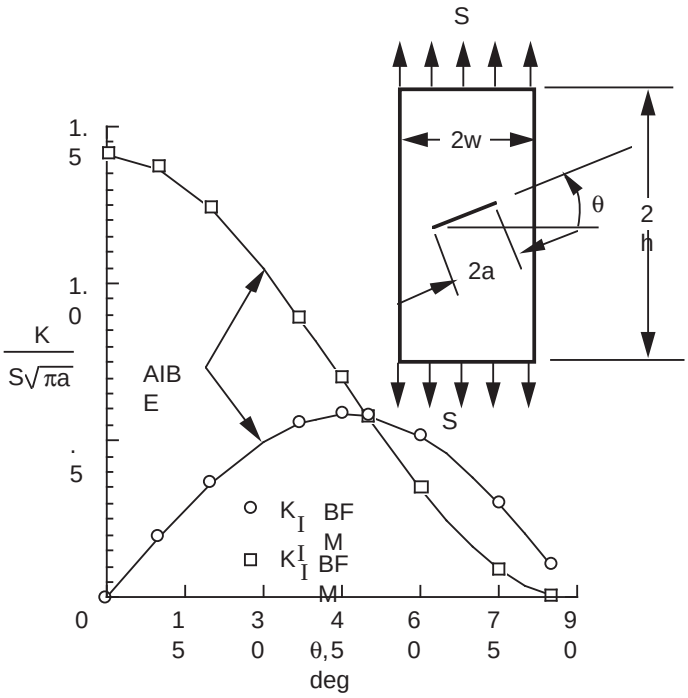

Figure 12. Normalized stress intensity factor for a single centered crack in a finite body, with the crack orientated at an angle θ ($\theta = 0°$ being perpendicular to the direction of loading) $h/w = 2$; $a/w = 1/3$.

the AIBE code and the BFM boundary force code (ref. 3). The AIBE boundary mesh was the same as that used in the analysis of the CCT configuration, and the crack mesh consisted of 12 elements oriented at an angle θ. The BFM mesh contained roughly the same number of elements. The two methods agreed within 0.7 percent for the mode I stress intensity factor and 0.3 percent for the mode II stress intensity factor, as shown in figure 12.

The next configuration analyzed was that of two collinear cracks in a finite plate. The cracks were oriented perpendicular to the direction of loading and located along the centerline of the specimen, as shown in figure 13. The length of both cracks was held constant ($a/w = 0.0625$) and the distance between them ($2d$) was varied. The stress intensity factors were calculated with the AIBE code and the FRANC finite element code (ref. 11). The AIBE boundary mesh was the same as used in the earlier examples, and each crack mesh consisted of 12 elements. Because of symmetry, the finite element mesh modeled one quarter of the specimen and consisted of 475 6-noded triangular elements. The stress intensity factor results of the two methods agreed within 1 percent, as shown in figure 14.

Stress Intensity Factor Hole Correction Verification

The use of a correction factor for the stress intensity factor was examined by comparing the stress

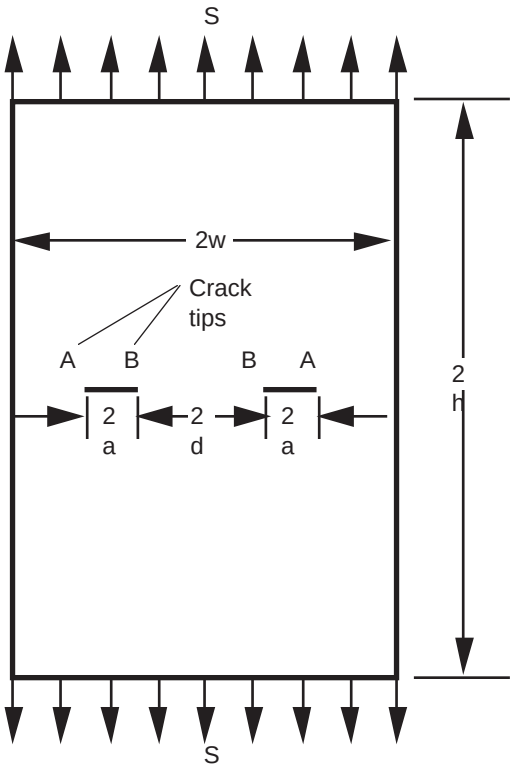

Figure 13. Illustration of multiple crack configuration used in the stress intensity factor verification. $h/w = 2$; $a/w = 0.0625$.

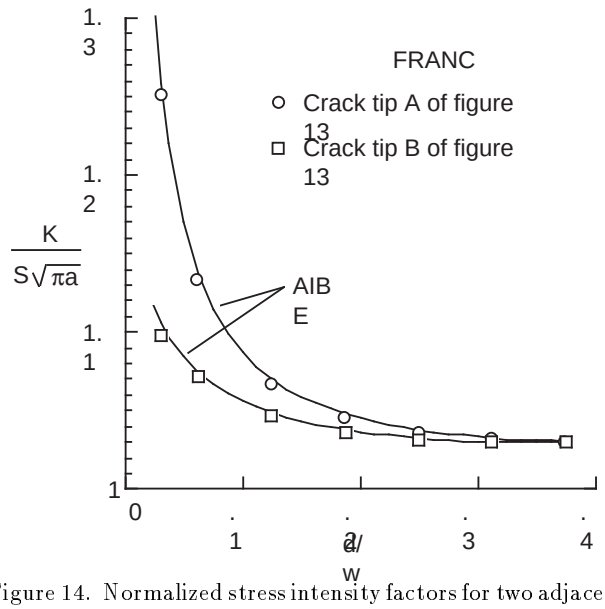

Figure 14. Normalized stress intensity factors for two adjacent cracks ($a/w = 0.0625$) in a finite body.

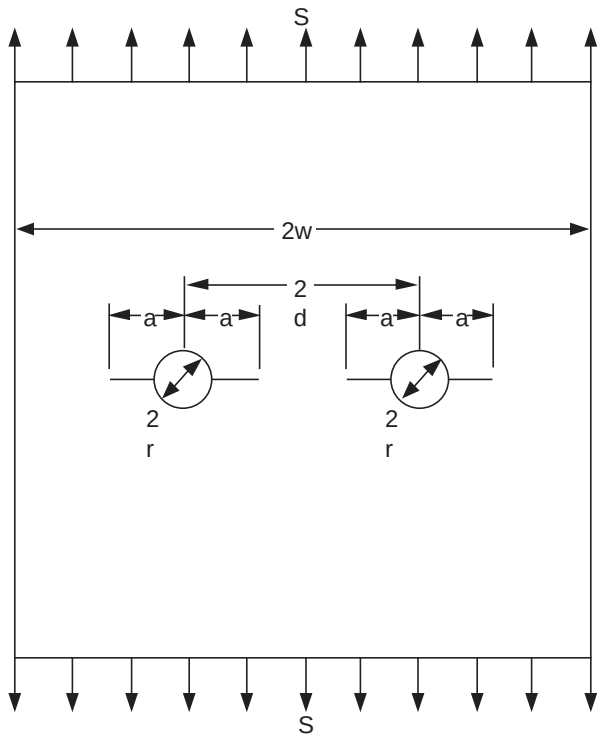

Figure 15. Illustration of the multiple open hole with cracks configuration used in the stress intensity factor verification. $r/d = 0.15$; $r/w = 0.0125$.

intensity factor calculated from the AIBE technique with the hole correction factor with results from a finite element analysis. The configuration considered was that of cracks propagating from two holes in a finite plate, as shown in figure 15. The AIBE program calculated the stress intensity factor for the two cracks in a finite plate. This solution was multiplied by the hole correction factor for cracks propagating from an open hole (eq. (29)). The stress intensity factor for either of the two inner crack tips calculated by the AIBE analysis with and without the hole correction factor is compared with results from the FRANC finite element code (ref. 11), as shown in figure 16. Because of symmetry, the finite element mesh modeled one quarter of the specimen and consisted of 444 6-noded triangular and 8-noded quadrilateral elements. The stress intensity factor results from the AIBE method with the hole correction factor agreed within 1 percent with the finite element results, as shown in figure 16.

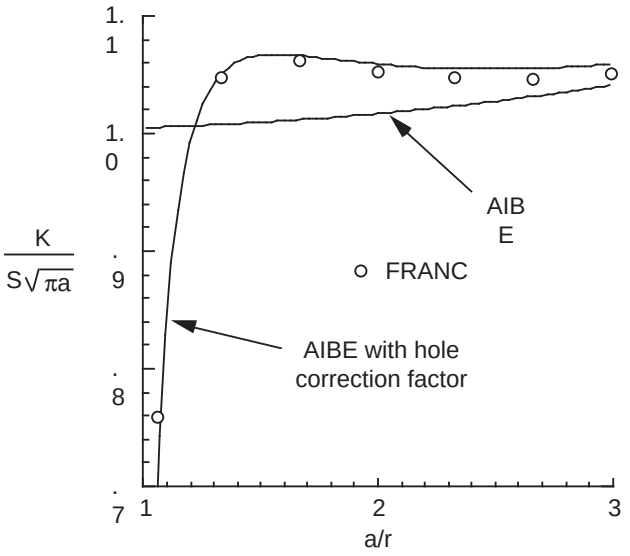

Figure 16. Stress intensity factor for the inner two crack tips shown in figure 15.

Experimental Procedure

MSD fatigue crack growth tests were conducted on five 304-mm-wide 2.29-mm-thick 2024-T3 aluminum alloy specimens subjected to remote uniform stress, as shown in figure 17. The specimens contained 10 holes, which were 3.8 mm in diameter and spaced 25.4 mm apart on centers. Cracks were developed by cutting small notches (0.7 mm long by 0.2 mm high) and cycling at the intended fatigue stress until distinct fatigue cracks were propagating from both sides of each hole. The experiments were conducted under constant amplitude loading (71 MPa) at a stress ratio of $R = 0.0$ and a frequency of 5 Hz. In three specimens (A6-02, A6-04, and A6-05) the center two holes were connected by a saw cut after precracking, as illustrated in figure 18, to simulate linkup of two adjacent cracks. The initial crack lengths after precracking are given in table I.

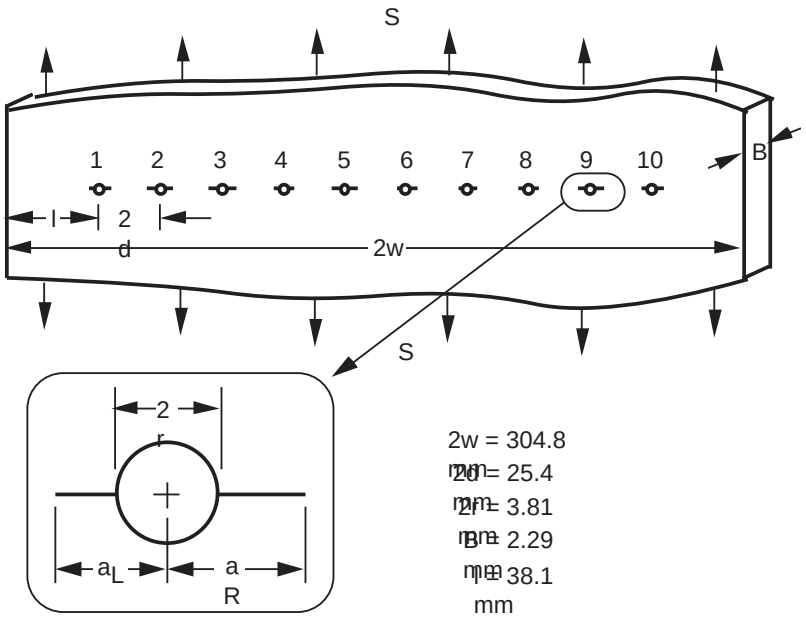

Figure 17. Schematic of the MSD cracking configuration.

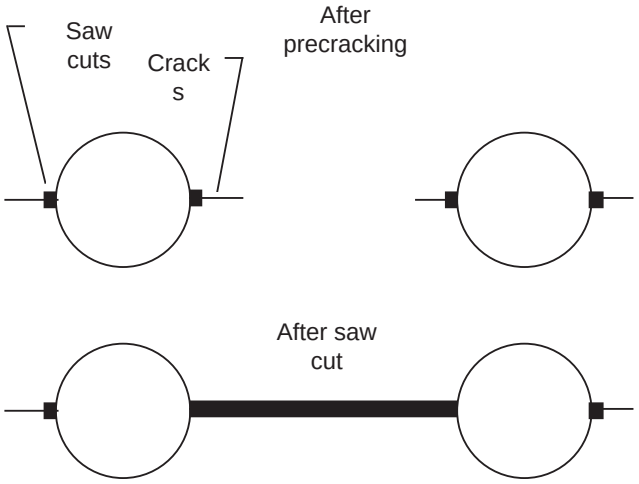

Figure 18. Illustration of saw cuts used to cause premature linkup of two adjacent cracks.

Life Prediction Procedure

Fatigue crack growth predictions require a description of the stress intensity factor and the baseline crack growth rate behavior. The stress intensity factors used in the predictions were obtained from the AIBE analysis with the correction factor for an open hole in an infinite plate for the configuration shown in figure 17.

Table I. Measured Initial Half Crack Length for the Constant Amplitude Fatigue Tests

Hole number	Crack tip	Crack length, mm				
		A6-01	A6-02	A6-03	A6-04	A6-05
1	a_L	2.90	3.61	2.84	2.82	3.48
1	a_R	2.87	3.02	2.62	3.23	2.95
2	a_L	3.25	4.52	3.00	3.63	5.08
2	a_R	3.25	4.19	2.31	4.34	4.09
3	a_L	3.63	3.30	3.99	4.75	3.23
3	a_R	3.63	3.45	3.96	5.18	2.84
4	a_L	2.62	3.48	3.51	5.16	3.15
4	a_R	2.62	3.76	2.90	5.13	3.05
5	a_L	3.15	16.0	3.76	17.0	16.2
5	a_R	3.15	*	2.34	*	*
6	a_L	2.57	*	2.41	*	*
6	a_R	2.57	16.0	3.33	17.0	16.2
7	a_L	2.39	3.15	4.62	3.51	3.25
7	a_R	2.39	2.74	4.06	3.53	3.45
8	a_L	2.46	2.69	2.77	3.96	3.28
8	a_R	2.44	2.82	3.48	4.04	3.20
9	a_L	3.30	3.45	3.84	3.89	3.73
9	a_R	3.30	3.76	5.08	3.78	3.94
10	a_L	3.00	2.79	2.97	2.95	3.10
10	a_R	3.00	3.30	3.51	3.43	3.81

*Linkup between adjacent cracks.

The baseline fatigue crack growth rate behavior for 2024-T3 aluminum used in the crack growth predictions was obtained from references 12 and 13 from constant amplitude tests on center crack tension specimens. The effects of fatigue crack closure were taken into account by calculating the crack opening stress S_o from an equation (ref. 14) based on a two-dimensional closure model (ref. 15), as given by

$$\frac{S_o}{S_{\max}} = A_0 + A_1 R + A_2 R^2 + A_3 R^3 \qquad (R \geq 0) \tag{32}$$

$$\frac{S_o}{S_{\max}} = A_0 + A_1 R \qquad (R < 0) \tag{33}$$

$$A_0 = \left(0.825 - 0.34\alpha + 0.05\alpha^2\right)\left[\cos\left(\frac{\pi S_{\max}}{2\sigma_o}\right)\right]^{1/\alpha} \tag{34}$$

$$A_1 = (0.415 - 0.071\alpha)\frac{S_{\max}}{\sigma_o} \tag{35}$$

$$A_2 = 1 - A_0 - A_1 - A_3 \tag{36}$$

$$A_3 = 2A_0 + A_1 - 1 \tag{37}$$

where

$S_{\max}$ maximum applied stress

R stress ratio (minimum stress/maximum stress)

σ_o flow stress (average between uniaxial yield stress and uniaxial ultimate tensile strength, 410 MPa for 2024-T3)

The constraint factor α simulates the three-dimensional constraint. A value of $\alpha = 1.73$ was found to be appropriate for 2024-T3 aluminum alloy ($B = 2.29$ mm) (ref. 15).

The crack opening stress, given by equation (32), was used to calculate an effective stress intensity factor range for the baseline crack growth rate data. The effective stress intensity factor range is given by

$$\Delta K_{\text{eff}} = \frac{\Delta K}{1 - R}\left(1 - \frac{S_o}{S_{\max}}\right) \tag{38}$$

Crack growth rate da/dN and effective stress intensity factor range ΔK_{eff} data were determined for use in the life predictions, as given by table II.

The life prediction started with the initial distribution of the 20 crack tips. The stress intensity factor and ΔK_{eff} were determined for each crack tip, and the crack growth rate da/dN obtained from the baseline behavior (table II). The crack tip with the largest crack growth rate $(da/dN)_{\max}$ was grown a fixed increment ($\Delta a = 0.12$ mm), and the required number of applied load cycles ΔN was determined as follows:

$$\Delta N = \frac{\Delta a}{da/dN_{\max}} \tag{39}$$

The crack growth increments for the remaining crack tips were determined from the number of applied load cycles as

$$\Delta a_i = \frac{da}{dN_i}\Delta N \tag{40}$$

where i is the crack tip number. The process was repeated until the net section stress was equal to the yield stress. The increments of applied load cycles ΔN were added to obtain the predicted cycles to failure N_p.

Table II. Effective Stress Intensity Factor Range Against Crack Growth Rate for 2024-T3 (refs. 12 and 13)

ΔK_{eff}, MPa-m$^{1/2}$	da/dN, m/cycle
1.42	3.56×10^{-10}
2.41	3.00×10^{-9}
3.29	6.10×10^{-9}
6.18	1.00×10^{-7}
10.95	4.32×10^{-7}
27.38	1.78×10^{-5}
49.29	2.54×10^{-4}

Life Prediction Results

The MSD fatigue tests were cycled to failure with optical crack length readings made periodically throughout the tests. The average initial half crack length and the observed cycles to failure are given in table III. The average half crack length was the sum of the tip-to-tip crack lengths divided by 20, regardless of whether any linkup of the cracks had occurred.

Table III. Summary of Constant Amplitude Fatigue Tests

Specimen ID	Average initial half crack length, mm	N_t Cycles to failure
A6-01	2.926	58 740
A6-02	*4.303	26 430
A6-03	3.368	46 210
A6-04	*4.864	15 600
A6-05	*4.400	25 920

*Holes 5 and 6 were connected by a saw cut.

As described above, life predictions were made for each specimen by using the baseline crack growth rate behavior given in table II, ΔK_{eff} calculated with equation (38), and the crack opening stress calculated with equation (32). The predictions, in terms of the ratio of predicted Np to test N_t cycles, are given in table IV. Three methods were used to calculate the stress intensity factor: AIBE, AIBE with the hole correction factor, and the solution for cracks propagating from a single hole in an infinite body. The AIBE method accounts for the boundary and crack interaction effects. The hole correction factor accounts for the effect of the hole without explicitly modeling each hole. The stress intensity factor solution for a hole neglects all crack interaction effects.

Table IV. Summary of MSD Fatigue Crack Growth Life Predictions

Test	Test type	Analysis method		
		Hole in infinite plate solution, N_p/N_t	AIBE only, N_p/N_t	AIBE with hole correction factor, N_p/N_t
A6-01	Nearly equal MSD	1.66	1.30	1.20
A6-02	Unequal MSD	1.46	0.93	0.93
A6-03	Nearly equal MSD	1.76	1.24	1.14
A6-04	Unequal MSD	2.10	1.13	1.13
A6-05	Unequal MSD	1.47	0.94	0.94
Average		1.69	1.11	1.07

The crack growth behavior for the two MSD tests with nearly equal initial crack lengths (no saw cut, A6-01 and A6-03) are shown in figures 19 and 20. The crack growth behavior of each of the 20 crack tips was predicted and the average crack length plotted as a function of the applied cycles. The fatigue crack growth predictions using the three stress intensity factor calculation methods are shown in both figures. Neglecting the crack interaction effects resulted in a prediction of the crack growth lives that was as much as 75 percent greater than observed. The AIBE method overpredicted the fatigue crack growth lives by as much as 30 percent, primarily because the holes will elevate the stress intensity factors when the cracks are small. The AIBE method with the hole correction factor gave the best predictions, predicting lives that were only 20 percent greater than the experimental results.

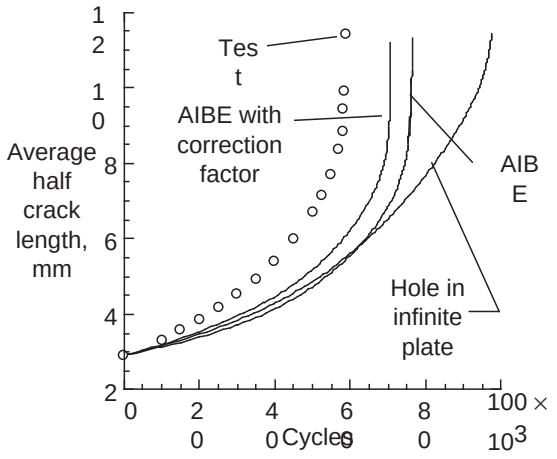

Figure 19. Predicted and actual fatigue crack growth behavior for MSD cracking test A6-01 (nearly equal MSD cracking).

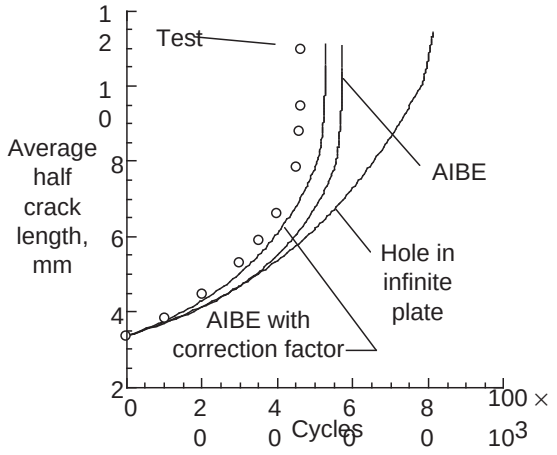

Figure 20. Predicted and actual fatigue crack growth behavior for MSD cracking test A6-03 (nearly equal MSD cracking).

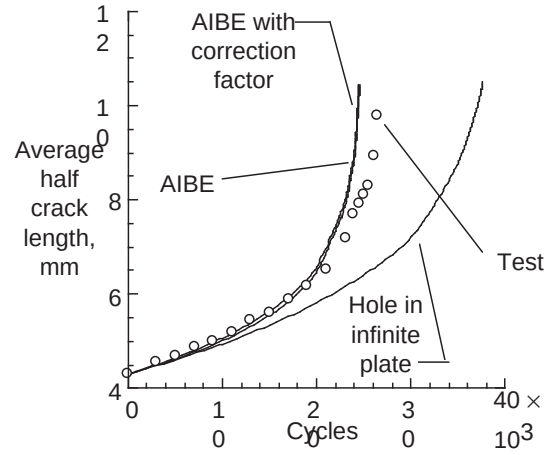

Figure 21. Predicted and actual fatigue crack growth behavior for MSD cracking test A6-02 (unequal MSD cracking).

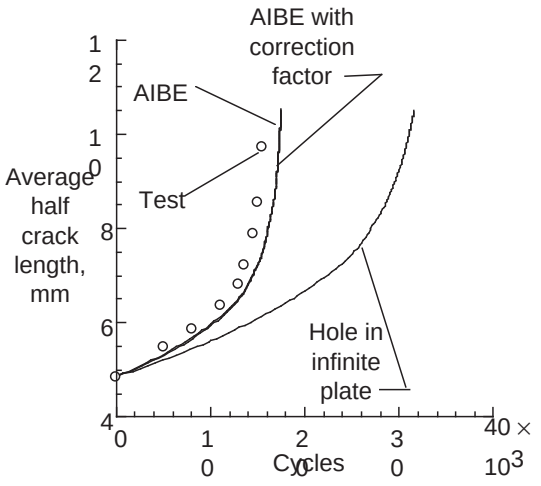

Figure 22. Predicted and actual fatigue crack growth behavior for MSD cracking test A6-04 (unequal MSD cracking).

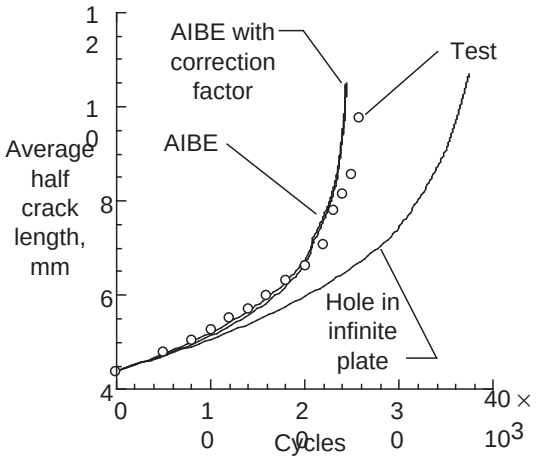

Figure 23. Predicted and actual fatigue crack growth behavior for MSD cracking test A6-05 (unequal MSD cracking).

The predictions of the crack growth behavior for the three MSD tests containing saw cuts to simulate crack linkup (unequal initial crack lengths, A6-02, A6-04, and A6-05) are shown in figures 21–23. The fatigue crack growth predictions made from the three methods are shown in comparison with the test results. The fatigue crack growth rates for the unequal MSD cracking tests were governed by the growth of the longest crack. The crack length was such that the hole had only a small effect on the stress intensity factor; thus, the AIBE method and the AIBE method with the hole correction factor gave about the same life. Neglecting the crack interaction effects overpredicted the lives by as much as 100 percent, primarily because of the crack interaction and linkup. The ratio of predicted to test life (N_p/N_t) is given in table IV for each of the tests.

Conclusions

The ability to evaluate the structural integrity of aircraft structures with multiple-site damage (MSD) is of great concern to the commercial transport aircraft industry. An efficient technique was developed to calculate stress intensity factors for multiple interacting cracks. The alternating indirect boundary element (AIBE) accurately models multiple interacting cracks and approximates the local structural details with a correction factor. This approach was verified through comparison of stress intensity factors calculated from accepted solutions, finite element methods, and boundary force analyses. The AIBE technique, in conjunction with a correction factor for cracks propagating from holes, was used to predict the fatigue crack growth life for multiple cracks propagating from a line of holes. The predictions were compared with experimental observations and the following conclusions were made:

- The AIBE analysis is an accurate method of calculating the stress intensity factors for multiple interacting cracks.
- The use of the AIBE analysis in conjunction with a local correction factor will result in accurate stress intensity factors for multiple interacting cracks propagating from local structural details such as holes.
- The fatigue crack growth life predicted from the AIBE analysis with a hole correction factor was within 20 percent of the experimentally observed life of tests conducted on flat panels with multiple cracks propagating from open holes.

NASA Langley Research Center
Hampton, VA 23681-0001
July 9, 1992

References

1. Paris, Paul C.; and Sih, George C.: Stress Analysis of Cracks. *Fracture Toughness Testing and Its Applications,* ASTM Spec. Tech. Publ. No. 381, c.1965, pp. 30–81.

2. Swenson, D. V.; Chih-Chien, C.; and Derber, T. G.: Analytical and Experimental Investigation of Fatigue in Lap Joints. *Advances in Fatigue Lifetime Predictive Techniques,* M. R. Mitchell and R. W. Landgraf, eds., Spec. Tech. Publ. 1122, American Soc. for Testing and Materials, 1991, pp. 449–459.

3. Tan, Paul W.; Raju, Ivatury S.; and Newman, James C., Jr.: Boundary Force Method for Analyzing Two-Dimensional Cracked Plates. *Fracture Mechanics: Eighteenth Symposium,* D. T. Read and R. P. Reed, eds., ASTM Spec. Tech. Publ. 945, c.1988, pp. 259–277.

4. Nishimura, Toshihiko; Noguchi, Yoshiharu; and Uchimoto, Tetsuo: Damage Tolerance Analysis of Multiple-Site Cracks Emanating From Hole Array. *J. Test. & Eval.*, vol. 18, no. 6, Nov. 1990, pp. 401–407.

5. Dawicke, D. S.; Poe, C. C, Jr.; Newman, J. C., Jr.; and Harris, C. E.: An Evaluation of the Pressure Proof Test Concept for Thin Sheet 2024-T3. *Theor. & Appl. Fract. Mech.,* vol. 14, no. 2, Nov. 1990, pp. 101–116.

6. Timoshenko, S. P.; and Goodier, J. N.: *Theory of Elasticity,* Third ed. McGraw-Hill Book Co., Inc., c.1970.

7. Westergaard, H. M.: Bearing Pressures and Cracks. *J. Appl. Mech.,* vol. 6, no. 2, June 1939, pp. A-49–A-53.

8. Tada, Hiroshi; Paris, Paul C.; and Irwin, George R.: *The Stress Analysis of Cracks Handbook.* Del Research Corp., c.1973.

9. Newman, J. C., Jr.: A Nonlinear Fracture Mechanics Approach to the Growth of Small Cracks. *Behavior of Short Cracks in Airframe Components,* AGARD-CP-328, Apr. 1983, pp. 6-1–6-26.

10. Brown, William F., Jr.; and Srawley, John E.; eds.: *Plane Strain Crack Toughness Testing of High Strength Metallic Materials.* ASTM Spec. Tech. Publ. No. 410, c.1966.

11. Wawrzynek, P. A.; and Ingraffea, A. R.: Interactive Finite Element Analysis of Fracture Processes: An Integrated Approach. *Theor. & Appl. Fract. Mech.*, vol. 8, no. 2, Oct. 1987, pp. 137–150.

12. Hudson, C. Michael: Effect of Stress Ratio on Fatigue-Crack Growth in 7075-T6 and 2024-T3 Aluminum-Alloy Specimens. NASA TN D-5390, 1969.

13. Phillips, Edward P.: The Influence of Crack Closure on Fatigue Crack Growth Thresholds in 2024-T3 Aluminum Alloy. Mechanics of Fatigue Crack Closure, J. C. Newman, Jr., and Wolf Elber, eds., Spec. Tech. Publ. 982, American Soc. for Testing and Materials, c.1988, pp. 505–515.

14. Newman, J. C., Jr.: A Crack Opening Stress Equation for Fatigue Crack Growth. *Int. J. Fract.*, vol. 24, no. 4, Apr. 1984, pp. R131–R135.

15. Newman, J. C., Jr.: A Crack Closure Model for Predicting Fatigue Crack Growth Under Aircraft Spectrum Loading. *Methods and Models for Predicting Fatigue Under Random Loadings,* J. B. Chang and C. M. Hudson, eds., ASTM Spec. Tech. Publ. 748, c.1981, pp. 53–84.